The Ocean Waveheight Nondirectional Spectrum from Inversion of the HF Sea-Echo Doppler Spectrum

DONALD E. BARRICK

NOAA/ERL/Wave Propagation Laboratory, Boulder, Colorado 80302

The measured HF sea-echo Doppler spectrum consists of prominent first-order peaks, around which exist second-order sidebands of a continuous nature. Theoretical models developed elsewhere are interpreted here and shown to satisfactorily account for these first and second-order measured spectral features. Employing these theoretical models, this paper derives a simple inversion technique for obtaining the waveheight nondirectional spectrum. The result is a closed-form expression, independent of the wave directionality factor, the radar look direction, or the stage of development of the waveheight spectrum. Approximations required in the derivation are stated along the way, and are shown to become increasingly valid in the limit of high seas and/or radar frequencies. The technique is tested by attempting to recover several input waveheight nondirectional spectra for various radar look directions. Comparisons show that the technique produces acceptable results for $k_o h > 0.2$, where k_o is the radar wavenumber and h is the rms waveheight. Application of the inversion technique to measured data is straightforward. One employs one of the stronger second-order Doppler sidebands (vs. Doppler frequency with respect to the first-order Doppler-peak frequency) and divides it by a parameterless, dimensionless weighting function derived in this paper. He then divides this result by the adjacent first-order spectral energy. The latter normalization (i) serves to remove any unknown radar path loss or system gain factors, and (ii) also eliminates the need for any *a priori* knowledge of the wave or radar directionality and/or the assumption of a model for these latter quantities.

1. Introduction

The use of HF radar to measure various parameters characterizing sea state was suggested by Crombie (1955) over two decades ago; he correctly deduced from measured echo spectra that the dominant (first-order) return was explained by the simple Bragg or diffraction-grating mechanism. More recently, analyses by Barrick (1972a, b) have developed theoretical models for the first-order sea echo which are compatible with Crombie's interpretations. Barrick (1971b, 1972b) extended these analyses to second-order, thereby accounting for the continuum in the observed Doppler spectrum between the first-order peaks; this theory reveals that a double (ocean) wave-wave interaction with the incident radar wave accounts for the scattered signal. Valenzuela (1974) obtained results that agree with those of Barrick, thereby lending credence to the conclusion that present models are correct to first and second order.

Hasselmann (1971) first suggested that the second-order Doppler sidebands ought to be proportional to the waveheight nondirectional temporal spectrum. He also suggested a convenient normalization of dividing these sidebands by the first-order echo, thereby canceling un-

known factors such as path loss and system gains. Stewart (1971) further explored conditions under which Hasselmann's hypothesis should be valid for a given sea-spectral model and radar-to-wind direction, deriving a result for mean-square waveheight. This paper derives precisely the relationships suggested by Hasselmann; no models for the waveheight directional spectrum are required, and the result is independent of the radar look direction. Approximations that are needed are stated along the way. These approximations—and their implicit requirements in terms of radar frequencies and sea roughness—are established by comparing nondirectional spectra recovered via our inversion technique with the original input to the model.

One can obtain many important descriptors of sea state from the waveheight nondirectional-spectrum, including rms waveheight, the dominant wind-wave period, swell periods, and the general stage of development of a wind-driven sea. This spectrum is readily obtained by oceanographers from time-series records of waveheight, as measured by wavestaffs or buoys with vertical accelerometers. (See Kinsman, 1965, for a general treatment of waves and their measurement.) The possibility of measuring this oceanographic quantity with skywave [over-the-horizon] or surface-wave HF radars (Barrick, 1973) represents an important step forward in replacing *in-situ* observing devices with remote-sensing techniques.

Results obtained in Barrick (1972a) show that the average, first-order sea-echo Doppler spectrum (for vertically polarized backscatter at grazing incidence), expressed as radar cross section per mean surface area per rad/s bandwidth, is:

$$\sigma_{(1)}(\omega_d) = 2^7 \pi k_o^4 \sum_{u,\ell} S_{\pm}(\kappa_{rx}, \kappa_{ry})\, \delta(\omega_d \mp \omega_{or}), \tag{1}$$

where $\bar{\kappa}_r$ is the total radar wavenumber vector, defined as $\bar{\kappa}_r \equiv \bar{k}_s - \bar{k}_i$. The coordinate system selected here has the backscattering wavevector, $\bar{k}_s$, taken at an angle ϕ with respect to the x-direction; hence the incidence radar wavevector, $\bar{k}_i$, lies in the direction $\pi + \phi$. Therefore, $\bar{\kappa}_r$ becomes $2k_o \cos\phi\,\hat{x} + 2k_o \sin\phi\,\hat{y}$, with k_o being the scalar radio wavenumber. The summation convention refers to the upper (u) and the lower (ℓ) subscripts and signs in the equation. The quantity ω_d is the radian Doppler shift of the received signal, defined as $\omega_d \equiv \omega_s - \omega_i$, with ω_s and ω_i being the frequencies of the scattered and incident signals, respectively. The deep-water gravity-wave dispersion relation is employed to define ω_{or}: $\omega_{or} = \text{sgn}(\kappa_{rx}) \times \sqrt{g\kappa_r} = \text{sgn}(\cos\phi)\,\omega_B$, where $\kappa_r = |\bar{\kappa}_r|$, g is the acceleration of gravity ($\sim 9.81\ \text{ms}^{-2}$), and ω_B is referred to as the first-order Bragg frequency ($\omega_B \equiv \sqrt{2gk_o}$). The expression sgn ($x$) is a sign indicator, which takes on the values ± 1 depending on whether x is $\pm$. The average waveheight directional spectrum—represented as S_+ and S_-—is defined and discussed in App. A; suffice it to say here that S_+ is defined to peak azimuthally along the $+x$-axis. The quantity $\delta(x)$ is the Dirac-delta function of argument x.

From Barrick (1972b), the corresponding result for second-order sea echo is

$$\sigma_{(2)}(\omega_d) = 2^8\pi_o^4 \sum\sum\iint_{u,\ell=-\infty}^{\infty} d^2\bar{\kappa}_I \, |\Gamma_T|^2 \, S_\pm(\kappa_{1x},\kappa_{1y})\, S_\pm(\kappa_{2x},\kappa_{2y})\, \delta(\omega_d \mp \omega_{o1} \mp \omega_{o2}), \tag{2}$$

where $\bar{\kappa}_1 \equiv 1/2\bar{\kappa}_r + \bar{\kappa}_I$; $\bar{\kappa}_2 \equiv 1/2\bar{\kappa}_r - \bar{\kappa}_I$;

$\omega_{o1} \equiv \text{sgn}(\kappa_{1x})\sqrt{g\kappa_1}$; $\omega_{o2} \equiv \text{sgn}(\kappa_{2x})\sqrt{g\kappa_2}$;

$\Gamma_T = \Gamma_H + \Gamma_{EM}$, where

$$\Gamma_H = -\frac{i}{2}\left[\kappa_1 + \kappa_2 + (\kappa_1\kappa_2 - \bar{\kappa}_1 \cdot \bar{\kappa}_2)\times \left(\frac{\omega_B^2 + \omega_d^2}{\omega_B^2 - \omega_d^2}\right)\frac{g}{\omega_{o1}\omega_{o2}}\right], \tag{3a}$$

$$\Gamma_{EM} = \frac{1}{2}(\kappa_{1x}\kappa_{2x} - 2\bar{\kappa}_1 \cdot \bar{\kappa}_2) / (\sqrt{\bar{\kappa}_1 \cdot \bar{\kappa}_2} + k_o\Delta), \tag{3b}$$

and where we take the integration variables here to be p, q, such that $\bar{\kappa}_I = p\hat{x} + q\hat{y}$. The quantity Δ is the normalized electrical impedance for the rough sea surface at grazing incidence, as defined and derived in Barrick (1971a).

The coupling coefficients Γ_H and Γ_{EM} are obtained from the second-order terms in the perturbational expansions for the sea waveheight and electromagnetic scatter, respectively; the equations describing these processes are nonlinear.

In the next section, we demonstrate how one can employ the waveheight directional spectrum in (1) and (2) to predict the average sea-echo signal spectrum as seen at the output of a receiver; this is then compared to measurements to establish the validity of the theoretical models. The third section shows and explains the approximation whereby one of the two waveheight spectrum factors appearing in (2) is removed from the integrand as a constant, while the remaining integral is evaluated. Sec. 4 discusses the approximation in which the coupling coefficient, Γ_T, is removed and evaluated at each Doppler shift, ω_d. Finally, Sec. 5 shows examples of the use of the complete inversion technique to recover input waveheight spectra to the theoretical model; thus the accuracy of the method is established for a variety of sea-state/radar-frequency conditions.

2. The Doppler Spectrum: Interpretation and Direct Solution

The preceding theoretical expressions show that the Bragg—or diffraction grating—effect is responsible for the scatter. Equation (1) shows that the ocean wavevector responsible for first-order backscatter is $\bar{\kappa}_r = \bar{k}_s - \bar{k}_i$; likewise the temporal wavenumbers follow the same first-order Bragg condition, i.e., $\omega_d = \pm\,\omega_B = \omega_s - \omega_i$. To second order, (2) shows that the two ocean wavesets responsible for scatter, having wavevectors $\bar{\kappa}_1$ and $\bar{\kappa}_2$, obey the relation $\pm\,\bar{\kappa}_1 \pm \bar{\kappa}_2 = \bar{k}_s - \bar{k}_i$, and the wave

frequencies are related as $\pm\omega_{o1} \pm \omega_{o2} = \omega_s - \omega_f$; thus two sets of ocean waves are interacting simultaneously to produce the scatter. Of course, the lowest-order dispersion equation relates ω_{of} to κ_f, and ω_{o1}, ω_{o2} to κ_1, κ_2.

By transforming (2) properly, the delta function in the integrand can be used to simplify the double integral, reducing it to a single integral. Of the various transformations possible, we have chosen one discussed in App. B. Its use results in the following expression for the second-order Doppler spectrum:

$$\omega_B \sigma_{(2)}(\omega_B \nu) = (2k_o)^8 \pi \nu^7 \sum_{\nu,\alpha} \sum \int_{\alpha_1}^{\alpha_2} \frac{d\alpha\, |\gamma_T(\nu,\alpha)|^2 S_\pm[\bar{\kappa}_1(\nu,\alpha)] S_\pm[\bar{\kappa}_2(\nu,\alpha)] \sin 2\alpha}{f^{16}(\alpha)\sqrt{2\nu^4 f^4(\alpha) - \nu^8 \cos^2 2\alpha - f^8(\alpha)}}, \tag{4}$$

where

$$\gamma_T(\nu,\alpha) = -\frac{i2f^4(\alpha)\nu^2}{\sqrt{\sin 2\alpha}} \left[\sqrt{2\sin 2\alpha}\,(\cos\alpha + \sin\alpha) + \mathrm{sgn}(\kappa_{1x})\mathrm{sgn}(\kappa_{2x})\left(1 + \sin 2\alpha - \frac{f^4(\alpha)}{\nu^4}\right)\times\right.$$

$$\left.\left(\frac{1+\nu^2}{1-\nu^2}\right)\right] + \left[\frac{4\nu^4 f^4(\alpha) - 3f^8(\alpha) - \nu^8 \cos^2 2\alpha}{\sqrt{f^4(\alpha) - \nu^4} + \Delta f^2(\alpha)/\sqrt{2}}\right].$$

with all of the remaining quantities being defined in App. B. The Doppler frequency is normalized here to the first-order Bragg frequency as follows: $\omega_d \equiv \nu\omega_B$.

One advantage of this transformation is that it explains a prominent feature of the Doppler spectrum: the peak at $\nu = 2^{3/4}$. This feature arises when the radical in the denominator of the second term of γ_T (i.e., the electromagnetic coupling factor) vanishes. Physically, the significance of this radical vanishing is that the intermediate radio wave interacting with the two sets of ocean waves having wavevectors $\bar{\kappa}_1$ and $\bar{\kappa}_2$ —which

has wavevector κ_I – is equal in magnitude to the free-space radio wavenumber, k_o, and is propagating along the surface. This means that the radio wave is at a transition point between being scattered and being evanescent; it therefore results in the greatest possible transport of (radio) energy between the two sets of ocean waves. The value of α, i.e., α_e, that causes the radical to vanish (νs ν) is that solution to the transcendental equation $f(\alpha_e) = \nu$; it is shown plotted in Fig. B-1. In this case, the peak at $\nu = 2^{3/4}$ is explained via our transformation by a simple "corner-reflector" effect. Two sets of ocean waves that produce intermediate scatter along the surface–as shown in Fig. 1–must propagate at angles α_e and $\pi/2$-α_e with respect to the backscatter direction. Furthermore, their wavelengths must be $L_1 = \pi/(k_o \cos\alpha_e)$ and $L_2 = \pi/(k_o \sin\alpha_e)$. From simple considerations, one can calculate the Doppler shift imparted by two such sets of ocean waves–both moving either toward or away from the radar–as $\nu = \pm[\cos^{1/2}\alpha_e + \sin^{1/2}\alpha_e]$. Now, as α_e varies, one sees that this expression has a maximum value–and in fact a point of mathematical stationarity–for $\alpha_e = 45°$, which occurs at $\nu = 2^{3/4}$. Thus two sets of waves at 45° with respect to the backscatter direction and 90° with respect to each other produce maximal intensity, as explained from elementary physics. This intensity manifests itself as a spectral peak at $\nu = 2^{3/4}$.

Before one launches into techniques for inverting the nonlinear integral equation, (4), to obtain the waveheight spectrum from the observed second-order Doppler spectrum, it is instructive to examine the numerical solution of the direct problem. Furthermore, the combination of the second-order echo with first-order, and their comparison with observations, should lend sufficient credibility to the entire theory that one could trust an inversion technique based upon these models. In order to perform such a numerical calculation, we employ a Phillips model for the spatial wavenumber spectrum, with a $\cos^4\theta/2$ directionality in azimuth. Thus we use

$$S_{\pm}(\kappa\cos\theta, \kappa\sin\theta) = \begin{cases} \dfrac{10^{-2}}{3\pi\kappa^4}\ \cos^4\theta/2 & \text{for } \kappa > \kappa_{co} = g/u^2 \\ 0 & \text{for } \kappa < \kappa_{co} = g/u^2, \end{cases} \tag{5}$$

where u is the wind speed in m/s. (This expression yields a rms waveheight $h = 0.05\ u^2/g$.) The above simplified model is only adequate for fully developed seas, that is, sea conditions where the wind duration is sufficient that the waves are in equilibrium with the wind. To obtain a result using (5) in (4), we assume as an example here that the radar looks in a direction $\phi = 45^\circ$ with respect to the dominant wave direction. Furthermore, we assume a radar operating frequency of 13.40 MHz ($k_0 = 0.281\ m^{-1}$). In order to combine the first-order Doppler spectrum with the second-order portion, we assume that the two pass through a radar receiver whose effective windowing width is 40 s (giving an effective Doppler resolution of .025 Hz). Finally, a wind speed of 25 knots (12.86 m/s is assumed, giving an rms waveheight in this case of 2.765 ft (0.843 m). The result is shown as the solid curve in Fig. 2.

Many HF Doppler spectra were measured in the 1972-1973 period with a multi-frequency radar on San Clemente Island; details of the measurements and equipment are found in Barrick et al. (1974). One typical set of three spectra (measured on three frequencies, 13.40, 13.41, and 13.43 MHz) are shown in Fig. 2 for comparison. A sample average of 9 independent 200-second Doppler spectra on each frequency were produced in this case, and then passed through the same 40-second windowing function as the theoretical spectrum. The observed wind speed was 25 knots, the seas were fully developed, and the radar beam looked in a direction of 50° with respect to the wind. Since path losses in a system such as this are always somewhat uncertain, the spectrum levels were adjusted until the first-order peaks were approximately aligned. The agreement of the second-order structures lends credibility to the models.

In general for this frequency range (5-30 MHz), the first-order peaks are constant in amplitude because they are sampling the sea spectrum in the saturated (equilibrium) region having κ^{-4} dependence. Hence, as waveheight and/or radar frequency increases, the second-order peaks of the spectrum increase both in their amplitudes and in their proximity to the first-order peaks. As the angle, ϕ, between dominant waves and radar varies between 90° and 0° or 180°, the shape of both portions of the Doppler spectrum varies between perfect symmetry about the carrier (at $\nu = 0$) to greatly skewed shapes in the $+\nu$ or $-\nu$ directions.

3. The Non-directional Spectrum Approximation

As a step in the inversion problem as postulated here, we show in this section that the integral

$$I_T = \sum_{u,\ell}\sum \int_{-\infty}^{\infty} dp \int_{-\infty}^{\infty} dq\ S_{\pm}(\kappa_{1x},\kappa_{1y})\ S_{\pm}(\kappa_{2x},\kappa_{2y})\,\delta\,(\omega_d \mp \omega_{o1} \mp \omega_{o2}), \tag{6}$$

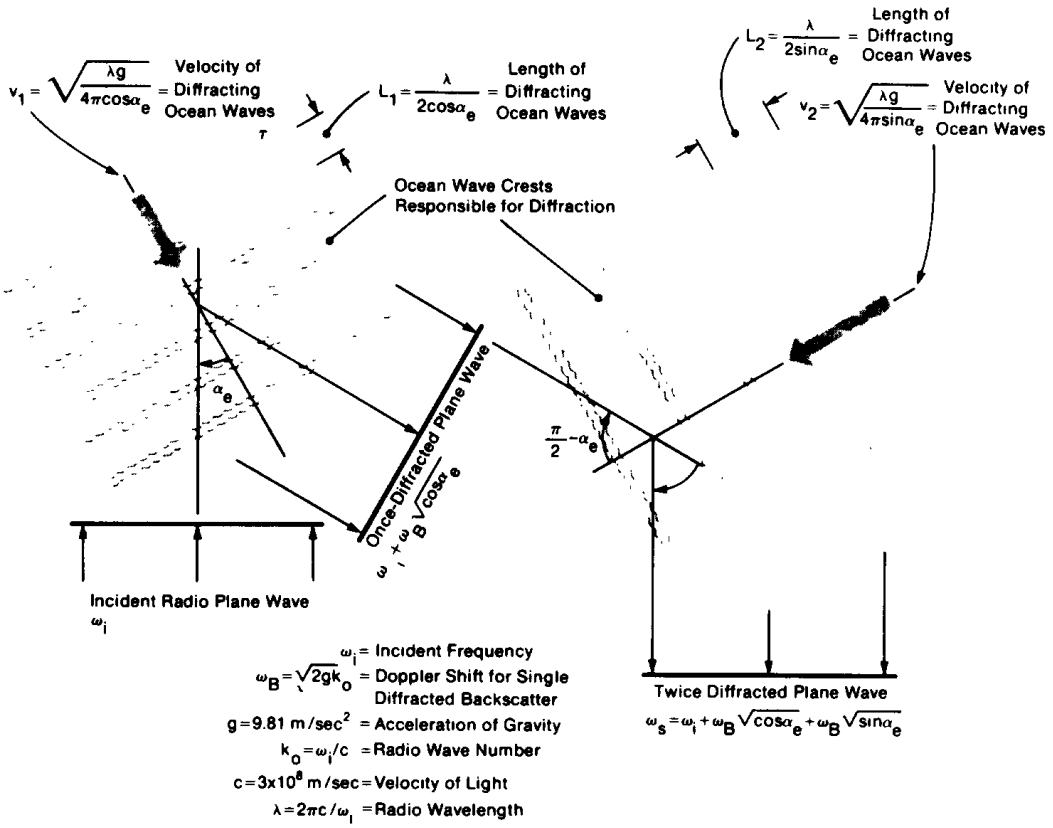

FIG. 1. Sketch showing second-order diffraction grating and Doppler effects when intermediate wave propagates along the surface.

can be approximated in terms of the waveheight non-directional spectrum when waveheight and/or radar frequency is large. Employing the same transformations outlined in App. B to derive (4) from (2), one can show that

$$\omega_B I_T = 8k_o^2 \nu^7 \sum_{\nu,\alpha} \sum \int_{\alpha_1}^{\alpha_2} \frac{d\alpha S_{\pm}[\bar{\kappa}_1(\nu,\alpha)]\, S_{\pm}[\bar{\kappa}_2(\nu,\alpha)] \sin 2\alpha}{f^4(\alpha)\sqrt{2\nu^4 f^4(\alpha) - \nu^8 \cos^2 2\alpha - f^8(\alpha)}} \cdot (7)$$

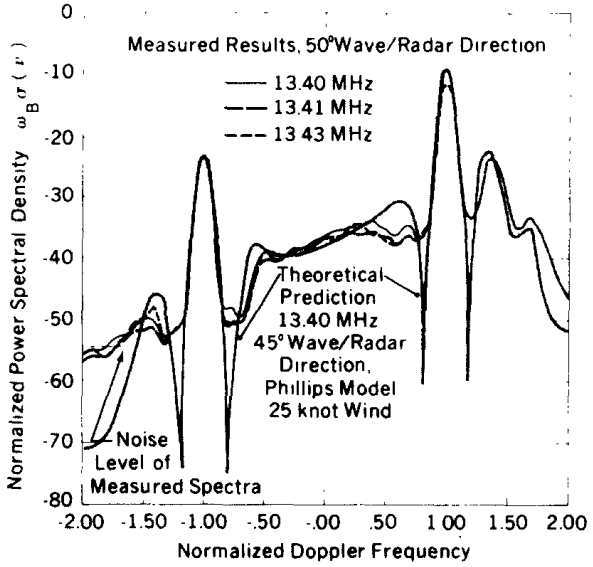

FIG. 2. Comparison of theoretical and experimental Doppler spectra (in decibels) at ∿13.4 MHz. Zero frequency corresponds to the carrier frequency position and ±1 corresponds to 0.374 Hz. Gausian smoothing is used on all curves.

Referring to Fig. B-1, the more heavily shaded regions near $\nu = \pm 1$ produce a much greater contribution to the integral than those farther removed; in this region, α is close to 0 and $\pi/2$. We plan to concentrate here only on simplification of the above integral in the region where ν is slightly greater than unity and α is near zero; results for the other seven corners follow by analogy. For $1 < \nu < 1.3$, one can see from Fig. B-3 that two product functionals contribute to the integral: $S_+(\bar{\kappa}_1)\, S_-(\bar{\kappa}_2)$ and $S_+(\bar{\kappa}_1)\, S_+(\bar{\kappa}_2)$. We will expand normalized frequency, ν, as $\nu \equiv 1 + \mu$ in this region, where the assumption to be made is that μ is small. Then we change variables twice, and arrive at an integral over the azimuthal angle, θ_2, of the second spectrum. This essentially results in the removal of the directional dependence of the waveheight spectrum, leaving the non-directioanl waveheight spectrum – evaluated at normalized temporal frequency μ – as being proportional to I_T for $\nu > 1$. In the process, all quantities will be expanded as series in μ, and all higher-order terms will be dropped. The error involved in this approximation for various radar frequencies and waveheight spectra will be examined in a subsequent section.

Higher sea states – characterized by large waveheights – result in smaller values of κ_{CO} (the spatial wavenumber near which most of the energy exists). Hence, for increasing sea states and/or radar frequency, the parameter β ($= 2k_O/\kappa_{CO}$) increases in size, and the dominant energy in the Doppler spectrum lies near $\mu=0$, $\alpha=0$. We will prove this here by deriving an approximation for μ_c in terms of β, where μ_c is the initial (normalized) frequency displacement from the Bragg line at which the Doppler energy begins to be significant. This is done by employing the Phillips cutoff relationship (the first of Eqs. (B-3)), eliminating α by employing (B-2), and expanding in a series of $\beta^{-n/2}$:

$$\mu_c = 1/\beta^{1/2} - 1/(2\beta) + 0(\beta^{-2}). \tag{8}$$

Thus for example, for $\beta=10$ (corresponding to an rms waveheight of 0.8 m and a radar frequency of 15 MHz for a fully developed sea), $\mu_c = 0.266$, which is reasonably small. At this point, the largest value of α is .09 rad or 5°; hence, for $\beta > 10$ the claim becomes increas-

ingly valid that the region of ν,α space which is important occurs for μ and α small. (Complementary symmetry would show that the same is true for μ and $\pi/2$-α small.)

Next we derive approximations for α_2 and α_1 (the α-integration limits) in this region in terms of μ; these expressions come from expanding the Jacobian of (B-2) in terms of (small) α and μ:

$$\alpha_1 \cong \mu^2(1-\mu)$$

and

$$\alpha_2 \cong \mu^2(1+\mu)\,. \qquad (9)$$

Thus α is indeed small even though μ may be only moderately small. Furthermore, the total excursion in α over this region of integration is even smaller, i.e., $2\mu^3$. We first use a transformation representing a linear shift in integration variables from α to δ, where $\delta \equiv \alpha - \alpha_1$; the integration limits on δ are now 0 and $2\mu^3$. Now expanding all quantities appearing explicitly in the integrand in terms of μ and δ, we retain only the lowest-order terms. As to orders of smallness, we note that $\delta \sim 0(\mu^3)$. Thus we find:

$$\kappa_{1x} \cong 2k_0\cos\phi \quad ; \quad \kappa_{1y} \cong 2k_0\sin\phi\,; \qquad (9a,b)$$

$$\kappa_{2x} \cong 2k_0[(\mu^2-\delta/\mu)\cos\phi \pm \sqrt{2\mu\delta-\delta^2/\mu^2}\,\sin\phi]\,; \qquad (9c)$$

$$\kappa_{2y} \cong 2k_0[(\mu^2-\delta/\mu)\sin\phi \mp \sqrt{2\mu\delta-\delta^2/\mu^2}\,\cos\phi]\,; \qquad \text{hence} \qquad (9d)$$

$$\kappa_1 \cong 2k_0;\ \kappa_2 \cong 2k_0\mu^2\,;\ \theta_1 \cong \phi\,; \qquad \text{and} \qquad (9e)$$

$$\theta_2 = \tan^{-1}\left[\frac{(\mu^2-\delta/\mu)\sin\phi \mp \sqrt{2\mu\delta-\delta^2/\mu^2}\,\cos\phi}{(\mu^2-\delta/\mu)\cos\phi \pm \sqrt{2\mu\delta-\delta^2/\mu^2}\,\sin\phi}\right]. \qquad (9f)$$

The other quantities in the integrand become

$$f^4(\alpha) \cong 1\ ;\ \sin 2\alpha \cong 2\mu^2\ ; \qquad (9g,h)$$

$$\sqrt{2\nu^4 f^4(\alpha) - \nu^8 \cos^2 2\alpha - f^8(\alpha)} \cong$$

$$2\sqrt{2\mu\delta - \delta^2/\mu^2}. \qquad (9i)$$

Our previous statement that one of the waveheight spectrum factors, $S_+(\bar{\kappa}_1)$ -which is common to both of the two terms in the integrand—can be removed from the integrand as a constant is now evident under these approximations. Thus the integral contribution to I_T from this region of $\nu>1$, α near zero, can now be written as

$$\omega_B I^{\alpha\sim 0}_{\nu\sim 1+} = 8k_o^4\mu^2 S_\pm(2k_o\cos\phi, 2k_o\sin\phi)\times$$

$$\sum_{\mu,\ell} \int_0^{2\mu^3} S_\pm[\bar{\kappa}_2(\mu,\delta)] \frac{d\delta}{\sqrt{2\mu\delta - \delta^2/\mu^2}}. \qquad (10)$$

At this point, we make a final transformation to an integration over θ_2. Note that our initial representation in p-q space mapped doubly onto the allowed regions of ν-α (or μ-δ) space. Thus, going back to κ_2, θ_2, we see from (9f) that the selection of one set of signs covers only half the total possible variation of θ_2 (from 0 to 2π). For example, using the upper signs, we see that at $\delta=0$, $\theta_2=\phi$, at $\delta=\mu^3$, $\theta_2=\pi/2+\phi$, and at $\delta=2\mu^3$, $\theta_2=\pi+\phi$. The lower sign choice covers the remaining region $\phi-\pi<\theta_2<\phi$, as δ varies between its limits 0 to $2\mu^3$.

Using the upper sign choice and the Jacobian

$$d\theta_2 = \frac{d\delta}{\mu\sqrt{2\mu\delta - \delta^2/\mu^2}} \quad \text{gives} \qquad (11)$$

$$\omega_B I^{\alpha\sim 0}_{\nu\sim 1+} = 8k_o^2\mu^3 S_+(2k_o\cos\phi, 2k_o\sin\phi)\times$$

$$\sum_{\mu,\ell} \int_{\phi}^{\phi+\pi} S_\pm(2k_o\mu^2\cos\theta_2, 2k_o\mu^2\sin\theta_2)\, d\theta_2. \qquad (12)$$

This is the desired result, for it shows that the approximations permit one to integrate out the angular dependence in the waveheight directional spectrum. Noting from App. A that by definition S_+ and S_- are symmetric, we can relate the integral to the nondimensional temporal spectrum using (A-6), (A-7), and (A-8), obtaining

$$I^{\alpha\sim 0}_{\nu\sim 1+} = \frac{1}{2} S_+(2k_o\cos\phi, 2k_o\sin\phi) S_t(\omega_B\mu). \qquad (13)$$

Up to now, we have considered only the contribution to I_T from the region near $\alpha=0$ (for $\nu>1$); an identical expression is obtained for the region near $\alpha=\pi/2$ ($\nu>1$). Hence we must double the above result to account for the total integral over α for $\nu>1$:

$$I_{\nu>1} = S_+(2k_o\cos\phi, 2k_o\sin\phi) S_t(\omega_B\mu). \qquad (14)$$

By analogy, one can derive an identical result for the region of ν slightly less than 1, defining in that case $\mu\equiv 1-\nu$. Finally, comparable results for the region of ν slightly greater and less than -1 give the same result as (14), but with S_+ replaced by S_-.

4. The Weighting-Function Approximation

Eq. (6) is similar—but not identical—to the second-order sea-echo Doppler spectrum as given in (2). Aside from multiplicative constants, it differs only in the presence of $|\Gamma_T|^2$ in the integrand of (2). The approximation to be made in this section involves the removal of $|\Gamma_T|^2$ from the integrand.

Let us refer to (4) and compare it with (7). Here, the non-common integrand factor is $2^5 k_0^6 \pi |\gamma_T(\nu,\alpha)|^2 / f^{12}(\alpha)$. For a given Doppler frequency, ν, this factor weights the remaining integrand over α. The simplest approximation would be to remove this factor and treat it as a constant, as though it varies neither with ν nor with α. Our approximation will be somewhat better. We will retain the ν-dependence of the factor, and then average it over α. Thus, the approximation goes as follows:

$$\omega_B \sigma_{(2)}(\omega_B \nu) = 2^5 k_o^6 \pi \overline{[|\gamma_T(\nu,\alpha)|^2 / f^{12}(\alpha)]}_\alpha \times$$

$$8 k_o^2 \nu^7$$

$$\Sigma\Sigma_{\nu,\alpha} \int_{\alpha_1}^{\alpha_2} \frac{d\alpha S_\pm [\bar{\kappa}(\nu,\alpha)] S_\pm [\kappa_2(\nu,\alpha)] \sin 2\alpha}{f^4(\alpha)\sqrt{2\nu^4 f^4(\alpha) - \nu^8 \cos^2 2\alpha - f^8(\alpha)}}, \quad (15)$$

$$\text{or } \sigma_{(2)}(\omega_B \nu) = 2^5 k_o^6 \pi w(\nu) I_{\nu>1} =$$

$$2^5 k_o^6 \pi w(\nu) S_+ (2k_o \cos\phi, 2k_o \sin\phi) S_t(\omega_B \mu), \quad (16)$$

where we have used (7) and (14), and we define the "weighting function", $w(\nu)$, as follows

$$w(\nu) \equiv \overline{[|\gamma_T(\nu,\alpha)|^2 / f^{12}(\alpha)]}_\alpha$$

$$= \frac{1}{\alpha_2 - \alpha_1} \int_{\alpha_1}^{\alpha_2} \frac{d\alpha\, |\gamma_T(\nu,\alpha)|^2}{f^{12}(\alpha)}, \quad (17)$$

and where we again note that for $\nu > 1$, $\mu \equiv \nu - 1$.

Thus we have derived an approximation whereby the waveheight non-directional temporal spectrum is expressed in terms of the second-order Doppler spectrum divided by a weighting function; the latter quantity is readily determined by performing the integration (numerically) of the theoretical coupling coefficient, $|\gamma_T|^2 / f^{12}(\alpha)$.

Figure 3 shows a plot of the weighting function numerically evaluated for $0 < \nu < 2.4$. (It is symmetric for $\nu < 0$.) Also shown are the contributions to $w(\nu)$ from the square of each of the two terms of $\gamma_T(\nu,a)$ taken separately. This permits one to obtain a feeling for where over ν the hydrodynamic second-order effects dominate the electromagnetic second-order effects, as expressed separately by w_h and w_e. Notice that w_e—and hence w—have peaks at $2^{1/2}$, $2^{3/4}$, and increase toward infinity as $\nu \to 0, \infty$. These characteristics will tend to correct the Doppler sidebands bringing their behavior more in line with the actual waveheight temporal spectrum that produced the Doppler sidebands.

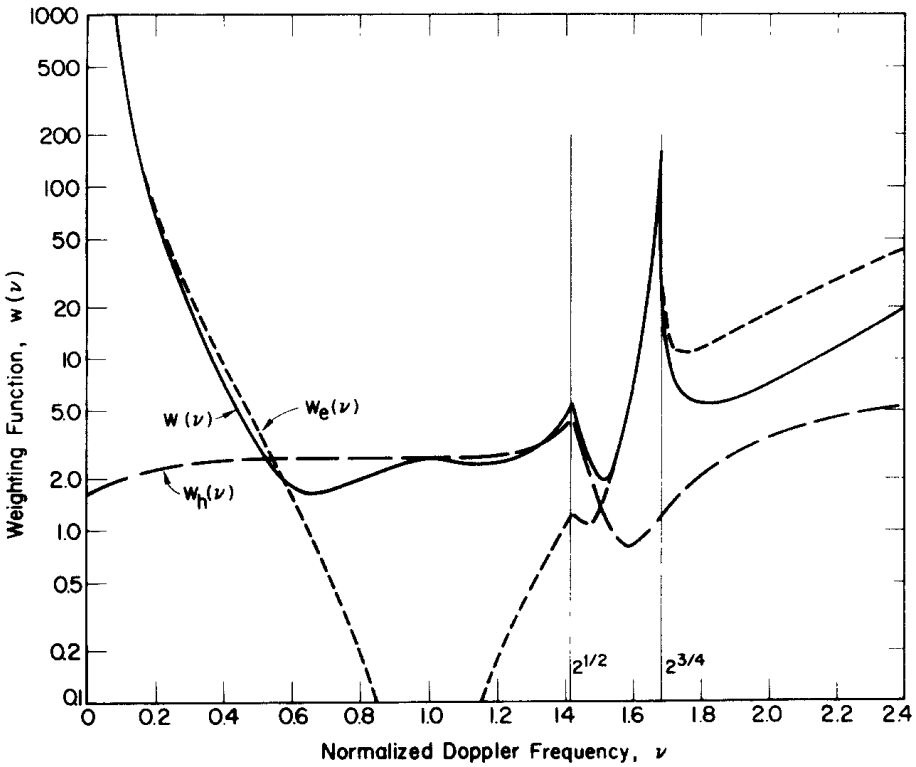

FIG. 3. Weighting function $w(\nu)$ as defined in (17). Also shown are the contributions to this function of the electromagnetic (e) and hydrodynamic terms (h) when each acts alone.

5. Application and Evaluation

Equation (16) contains the directional waveheight spatial spectrum, $S+$, evaluated at the Bragg wavenumbers $2k_0\cos\phi$, $2k_0\sin\phi$. It is a simple matter to remove this factor by noting that it appears in the expression for first-order scatter, Eq. (1). Integrating (1) over positive Doppler frequencies ($\nu>0$), and assuming $\phi<\pi/2$, we obtain

$$\int_0^\infty \sigma_{(1)}(\omega_d)\,d\omega_d$$

$$= 2^7\pi k_0^4 S_+(2k_0\cos\phi, 2k_0\sin\phi). \qquad (18)$$

Hence for $\nu>0$, we have (using $\omega_d\equiv\omega_B\nu$):

$$S_t[\omega_B|\nu-1|] = \frac{4\sigma_{(2)}(\omega_B\nu)/w(\nu)}{k_0^2\int_0^\infty \sigma_{(1)}(\omega_B\nu)\,d(\omega_B\nu)}. \qquad (19)$$

When dealing with measured data, this result says the following. If one can isolate the dominant first-order Doppler peak, one simply integrates this portion of the power spectral density to obtain the total first-order energy. Either of the second-order sidebands near that first-order peak is then divided by this first-order quantity, af-

ter the second-order sideband has itself been divided by the weighting function calculated here. This expression is self-normalizing, because any unknown path-loss or system constants multiplying the entire Doppler spectrum will cancel in the division process.

The ultimate worth of any inversion technique such as this will be established by comparing radar measurements with exact "sea-truth" data for the waveheight temporal spectrum. Until such measurements can be made, we can obtain a feel for the validity of the approximation behind this inversion by starting with a given form for the waveheight temporal spectrum, employing the theory here to calculate the average first and second-order Doppler spectra, and then inverting them via (19), attempting to recover the original waveheight spectrum. The magnitude of the departure of the recovered from the original waveheight spectra gives an indication of the quality and regions of validity of the approximations.

To illustrate the accuracy of the technique, we employ the classic ω^{-5} Phillips model for the waveheight temporal spectrum and give it a $\cos^4\theta/2$ directional dependence; this is expressed in (5). In particular, we choose three radar directions (with respect to the dominant wave directions): $\phi = 0$, 45°, and 90°. Finally, we employ a "sharp" lower-end cutoff, as well as a truncated or flat-topped lower end[1]. The parameter β is the ratio $2k_o/\kappa_{co}$, where κ_{co} is the actual lower-end cutoff. In the case of the truncated spectrum, the flat top extends from cutoff, ω_{co} ($\omega_{co} = \sqrt{g\kappa_{co}}$) out to $\sqrt{2\omega_{co}}$. In employing (19) to recover S_t, both Doppler sidebands near the dominant first-order peak (at $\nu=+1$) were used; they were added and halved to obtain an average. Figures 4 and 5 show the comparisons between the recovered and the original spectra.[2]

Qualitative comparison of the shapes of the recovered vs input spectra—when done on semi-logarithmic graphs as in Figs. 4 and 5—leaves some doubt as to the exact accuracy of the technique. A meaningful quantitative comparison is the relationship between the areas under the curves. This area is in fact the mean-square waveheight of the sea, perhaps the single most important descriptor of sea state. Let us denote by h_* the rms "radar-deduced" waveheight as recovered using the inversion technique based upon the area under the gray curves, and h, the rms waveheight from the input spectral model. Then Table 1 summarizes the ratio h/h_* for the models represented in Figs. 4 and 5; unity represents a perfect recovery. Further detailed

[1] Although many other shapes have been proposed for the waveheight spectrum, we frequently observed nondirectional spectra with our Waverider buoy during the San Clemente Island experiments which closely resembled the models used here. The model with the "sharp" lower-end cutoff appeared more characteristic of fully-developed seas, while the truncated or "flat-topped" model was often seen in seas which were not yet fully developed by the wind.

[2] To provide some feel for the parameter β, if we take 15 Mhz (a typical HF radar frequency), for $\beta/2=4$ and 10, we obtain rms waveheights of 0.636 m and 1.592 m for the sharp spectrum, with 0.469 m and 1.173 m for the truncated spectrum.

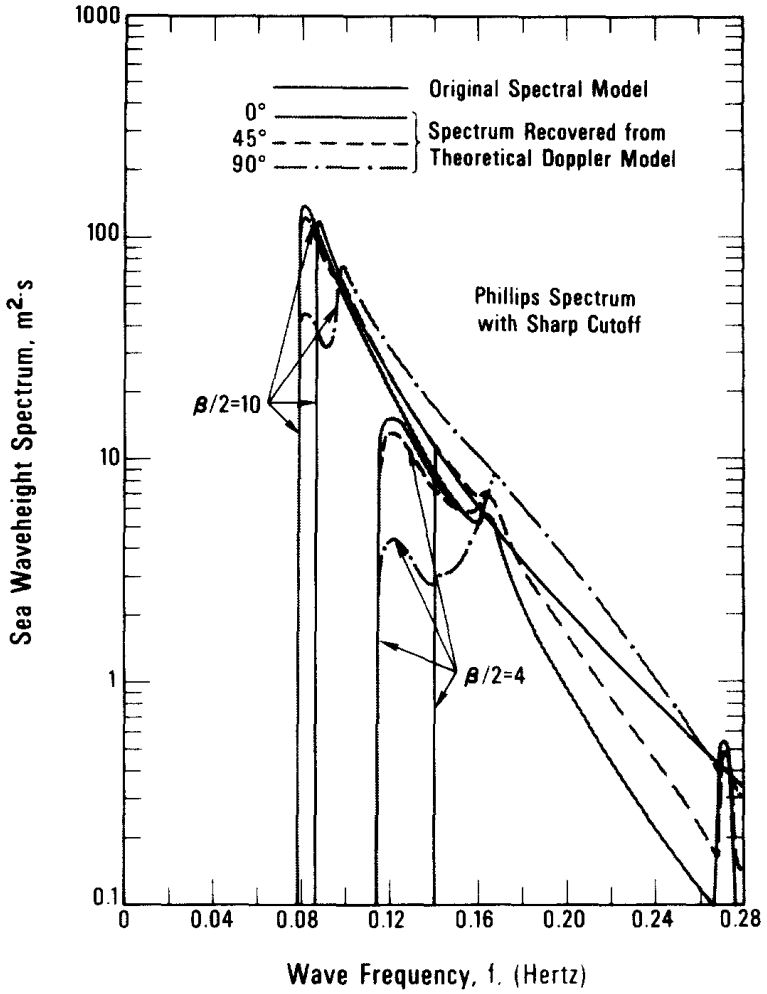

FIG. 4. Comparisons between input (original) and output (recovered) waveheight temporal spectra obtained from inversion result (19) for three different radar/wind directions. Phillips model with sharp cutoff is used as input.

studies of waveheight extraction and comparisons with measured data are found in Barrick [1977].

As one can see from Figs. 4 and 5 and Table 1, the quality of the approximation improves for increasing seas and/or frequency, as represented by increasing β. For remote-sensing applications, this is a satisfying trend, since accuracy is probably least important for low seas. Likewise, observe that the ω^{-5} dependence of the input spectrum is best recovered at the lower end representing the longer, higher waves. Notice also that the singularities which occur in the Doppler spectrum at $2^{1/2}$ and $2^{3/4}$ are effectively removed by the use of the weighting function, helping thereby to recover the original shape of the waveheight spectrum.

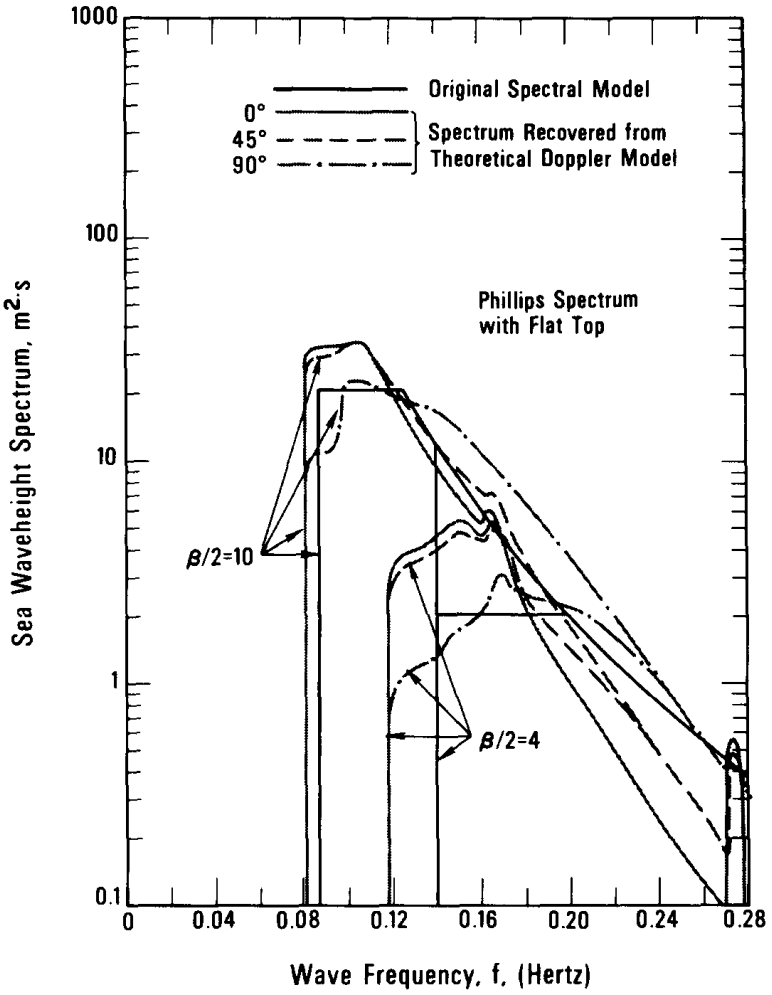

FIG. 5. Comparisons between input (original) and output (recovered) waveheight temporal spectra obtained from inversion result (19) for three different radar/wind directions. Phillips model with flat top is used as input

6. Conclusions

Ever since the solution relating the second-order HF Doppler sea echo to the integral of the product of two waveheight directional spectra appeared over five years ago, it has been evident that one should be able to sense many waveheight parameters with a single radar observation from a single direction. Published works to this time have mainly been concerned with the direct problem, i.e., given a waveheight spectral model, calculate the received Doppler spectrum. Such an approach – while it has permitted verification of the theoretical model – has limited application to remote sensing, for it requires a person to estimate wave characteristics by selecting from many the one precomputed Doppler

TABLE 1
h/h*

	Radar/wind direction		
	0°, 180°	45°, 135°	90°
Sharp cutoff			
$\beta/2=4$	0.848	0.833	0.901
$\beta/2=10$	0.870	0.851	0.923
Flat top			
$\beta/2=4$	0.827	0.824	0.940
$\beta/2=10$	0.880	0.856	0.913

pattern that most nearly matches his observations.

The ultimate goal should be derivation of an exact inversion scheme for the nonlinear integral eq. (2). A step in this direction is Lips' recent work (1977). We have produced the derivation of a simple closed-form solution, which is based upon Hasselmann's suggestion (1971) that the second-order Doppler sidebands ought to replicate in some sense the nondirectional waveheight temporal spectrum. Our derivation involves the calculation and normalization of the second-order Doppler spectrum by a simple, dimensionless weighting function, calculated and presented here. Our technique has the advantage that no model—either for the directional or for the radial portions—need be assumed for the waveheight directional spectrum appearing (twice) in the integrand, as seen from the theory. Although we chose to illustrate the accuracy of the inverted results in this paper by employing specific models having (i) abrupt lower-end cutoffs, with both sharply peaked and flat radial wavenumber shapes, and (ii) a $\cos^4(\theta/2)$ angular dependence, we have tested the technique against a variety of other models. These include spectra whose radial wavenumber dependence follows empirical models near the lower end suggested by Neumann and Pierson, Pierson and Moskowitz (Kinsman, 1965), and whose angular dependence has both the semi-isotropic nature suggested by Phillips (1966) (i.e., no waves opposing the wind) and for $\cos^s(\theta/2)$ models with s as high as 16. The inversion results there have identical trends and accuracies as those presented here; they are omitted for lack of space. These additional case studies do support the claim that the inversion technique is indeed general, and does not depend upon a given model behavior for the waveheight directional spectrum.

By employing our result to recover various waveheight nondirectional spectra used to calculate the Doppler spectrum, we have determined that the approximations leading to our result are valid under conditions of higher seas and/or radar frequencies. Both the magnitude, shape, and area of the recovered curves resemble those of the original waveheight spectrum under these conditions, with only slight differences depending upon the radar direction with respect to the dominant

wave direction. In particular, if one defines a parameter k_0h, where k_0 is the radar wavenumber and h is the rms waveheight, our comparisons show that reasonable agreement can be expected when this parameter exceeds 0.2.

Having obtained the non-directional waveheight spectrum from measurements in this manner, one can establish many important descriptors of the sea state, such as rms waveheight, the dominant wave period, the presence and frequency of any swell components, and the stage of development of a wind-driven sea.

HF surface-wave radars can regularly produce Doppler spectra with sufficient resolution that the first-order and second-order components can be clearly recognized and used with this approach. However, skywave radar Doppler spectra will frequently be "smeared" by ionospheric multipath effects so that it will not always be possible to readily distinguish the first from the second-order energy. In such cases, direct application of the technique derived here will not be possible without further refinements and approximations.

Acknowledgments

The author wishes to acknowledge helpful and continuing discussions with Dr. Bob L. Weber of our laboratory, and appreciates the very useful comparisons of methodologies and results with those of Dr. Belinda J. Lipa of Stanford University.

Appendix A. The Waveheight Spatial-Temporal Spectrum

We define our coordinates such that the +x-direction coincides with the azimuth along which the traveling ocean waves have maximum strength; otherwise, the waveheight spatial spectrum can have a completely arbitrary angular distribution. We assume that in general waves moving in the back half-space (i.e., with a velocity component along the -x- direction) can exist. Furthermore, we employ the lowest-order dispersion relation for first-order ocean waves. Finally, with the requirement that the ocean waveheight be a real number, we employ the following definition for the waveheight, ζ, as a function of space and time (where a Fourier-series representation is used over space):

$$\zeta(x,y,t) = \sum_{m,n=-\infty}^{\infty} P_+(m,n)\, e^{iamx+iany-i\omega\, mnt} + \sum_{m,n=-\infty}^{\infty} P_-(m,n)\, e^{iamx+iany+i\omega\, mnt}, \tag{A-1}$$

where $P_\pm(-m,-n) = P_\pm^*(m,n)$ and $\omega_{mn} = \text{sgn}\,(m)\sqrt{g[(am)^2 + (an)^2]^{1/2}}$, with "$a$" being a fundamental spatial frequency, assumed to be much less than the smallest wavenumbers actually present on the ocean. Here, $P_\pm$ describes the amplitudes of those waves having velocity components in the ±x-directions, respectively. We note that such a definition of real waves is required in all of the

perturbational scattering theories patterned after Rice (1951), where the real spatial waveheight series is extended to include time variation, as in Barrick (1972a).

The average spatial-temporal waveheight spectrum may now be defined in the following manner, where the Fourier coefficients are taken to be independent random variables:

$$S(\kappa_x,\kappa_y,\omega) = \frac{1}{(2\pi)^3}\iiint_{-\infty}^{\infty} <\zeta(x,y,t)\zeta(x+\tau_x,y+\tau_y,t+\tau_t)>\times$$

$$e^{\,i\kappa_x\tau_x - i\kappa_y\tau_y + i\omega\tau_t} d\tau_x d\tau_y d\tau_t$$

$$\equiv S_+(\kappa_x,\kappa_y)\,\delta(\omega-\omega_o) + S_-(\kappa_x,\kappa_y)\,\delta(\omega+\omega_o), \tag{A-2}$$

where $\omega_o = sgn\ (\kappa_x)\sqrt{g\kappa}$, with $\kappa = \sqrt{\kappa_x^2+\kappa_y^2}$ and $\kappa_x = am$, $\kappa_y = an$. In terms of the coefficient averages, we have

$$<P_\pm(m,n)P_\pm^*(k,l)> = \begin{cases} a^2 S_\pm(\kappa_x,\kappa_y) & \text{for } k=m,\ l=n; \\ 0 & \text{for other } k,l. \end{cases} \tag{A-3}$$

This definition requires the following normalization for mean-square waveheight:

$$h^2 = <\zeta^2(x,y,t)> = \iiint_{-\infty}^{\infty} S(\kappa_x,\kappa_y,\omega)\,d\kappa_x\,d\kappa_y\,d\omega = \sum_{u,l}\ \iint_{-\infty}^{\infty} S_\pm(\kappa_x,\kappa_y)\,d\kappa_x\,d\kappa_y. \tag{A-4}$$

Note also that because waveheight and its spatial correlation coefficient must be pure real, $S_+(-\kappa_x,-\kappa_y) = S_+(\kappa_x,\kappa_y)$, with an analogous symmetry requirement for S_-.

Oceanographers using tilt-buoys (Tyler et al., 1974) for measurements would define a waveheight directional spectrum in polar coordinates, $S_s(\kappa,\theta)$ (for a spatial spectrum) or $S_t(\omega,\theta)$ (for the temporal version) with the following interrelationships:

$$h^2 = \int_0^\infty d\kappa \int_{-\pi}^{\pi} d\theta S_s(\kappa,\theta) = \int_0^\infty d\omega \int_{-\pi}^{\pi} d\theta S_t(\omega,\theta); \tag{A-5}$$

$$\text{with} \quad S_t(\omega,\theta) = \frac{2\omega}{g} S_s\left(\frac{\omega^2}{g}, \theta\right) \tag{A-6}$$

from the dispersion relation, and the simple non-directional spectra defined as

$$S_s(\kappa) = \int_{-\pi}^{\pi} S_s(\kappa,\theta)\, d\theta \qquad S_t(\omega) = \int_{-\pi}^{\pi} S_t(\omega,\theta)\, d\theta. \tag{A-7}$$

The quantity $S_s(\kappa,\theta)$ is related to our spectrum as

$$S_s(\kappa,\theta) = \begin{cases} 2\kappa S_+(\kappa\cos\theta, \kappa\sin\theta) & \text{for } -\frac{\pi}{2} < \theta < \frac{\pi}{2}, \\ 2\kappa S_-(\kappa\cos\theta, \kappa\sin\theta) & \text{for } -\frac{3\pi}{2} < \theta < -\frac{\pi}{2}. \end{cases} \tag{A-8}$$

Attention is directed to frequent confusion involving a factor of two in relating oceanographically observed (Teague et al., 1975) or modeled (Barrick, 1972a) waveheight spectra to scattered sea echo. Scattering theory requires waveheight descriptions similar to (A-1), and hence waveheight spectra of a form (A-2); thus we must employ (A-8) to relate these to the oceanographic observables.

Appendix B. The Integral Transformation

Equation (2) for the second-order scatter can be reduced from a double to a single integral by employing the sifting property of the Dirac-delta function. While the left side of the equation is an explicit function of one independent variable, ω_d, the integrand is a function of three: ω_d, p, and q. The delta function implies an interdependence among the three such that only two are strictly independent; one of the two is then eliminated in the final single integration. To employ the delta function to eliminate one of the two integrals, one must transform variable from p and q to two other variables with a (generally) multivalued mapping. The choice of transformation variables is optional, and various investigators have made different selections. There are problems encountered in each method. Ours has the advantages that a cubic (or higher) equation does not arise within the delta function argument, and that the final integration limits are finite; the disadvantage is that these integration limits must be found by solving a transcendental equation (numerically) for each value of ω_d and θ.

Our transformation process goes basically as follows:

(a) $p,q \rightarrow \kappa_1, \kappa_2$ $(-\infty<p,q<\infty;\ \kappa_1,\kappa_2 > 0)$, where κ_1 and κ_2 are as defined following (2).

(b) $\kappa_1, \kappa_2 \rightarrow r,\alpha$ $(r>0;\ 0 < \alpha < \frac{\pi}{2})$, where $\kappa_1 \equiv r\cos\alpha$ and $\kappa_2 \equiv r\sin\alpha$.

(c) $r \rightarrow \eta$ $(-\infty < \eta < \infty)$, where $\eta \equiv \pm\ \omega_{01} \pm \omega_{02} = grf(\alpha)$, where $f(\alpha) \equiv \pm\ \mathrm{sgn}(\kappa_{1x})\cos^{1/2}\alpha \pm \mathrm{sgn}(\kappa_{2x})\sin^{1/2}\alpha$, the upper/lower sign choices depending upon which of the four terms of the integrand in (2) is being used.

The Jacobian of the *total* transformation process is

$$J(\eta,\alpha) = \frac{2\eta^7 \sin 2\alpha}{g^2 f^4(\alpha)\sqrt{8g^2 k_0^2 \eta^4 f^4(\alpha) - \eta^8 \cos^2 2\alpha - 16 g^4 k_0^4 f^8(\alpha)}} \qquad (B\text{-}1)$$

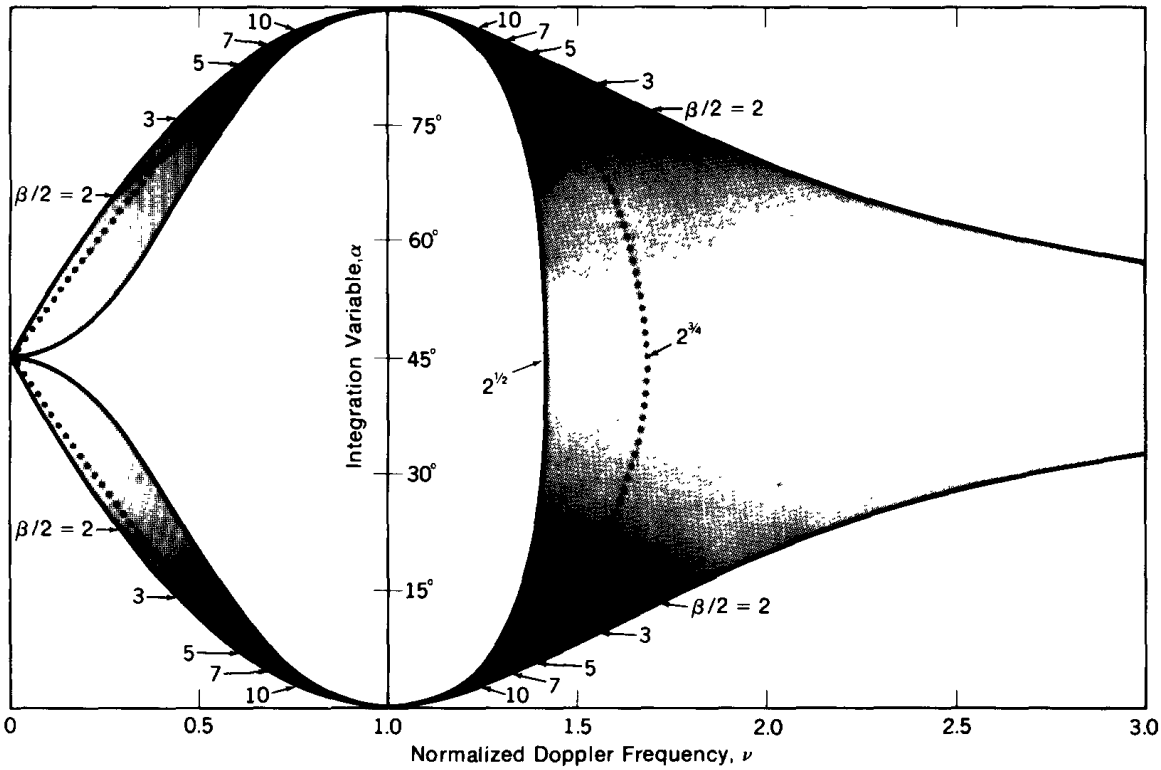

FIG. B-1. Plot showing regions over $\nu-\alpha$ space used for integration of (4). Solid lines delimiting regions of heavier shading are solutions to (B-3). Dotted lines indicate electromagnetic singularity, obtained as solution to equation $f(\alpha_e) = \nu$.

At this point the argument of the delta function becomes $\omega_d - \eta$; the integral over η is thus eliminated by dropping the delta function and replacing η everywhere by ω_d. With a further normalization of Doppler frequency ω_d as $\nu \equiv \omega_d/\omega_B$, one obtains (4).

Several details of this transformation must be outlined carefully. The first has to do with the integration limits on α. There are three types of limits:

(a) Jacobian-imposed limits. This limit is dictated by the fact that the argument of the radical in the denominator of J must be positive in order for the mapping to be real. In terms of ν, the inequality defining this limit, α_j, is

$$2\nu^4 f^4(\alpha_j) - \nu^8 \cos^2 2\alpha_j - f^8(\alpha_j) \geq 0. \quad \text{(B-2)}$$

(b) Spectral-model limits. Certain types of waveheight spectral models—such as the Phillips (1966) model—are nonzero by definition only when the wavenumber exceeds a lower cutoff value; for fully developed seas, this is often given in terms of wind speed, u, as $\kappa > \kappa_{co} = g/u^2$ (see Eq. (5) of the text.) Thus, for a model such as this, the integrand is nonzero only when κ_1 and κ_2 exceed this cutoff, giving rise to the inequalities

$$\nu^2 \cos\alpha_w / f^2(\alpha_w) \geq 1/\beta$$

and

$$\nu^2 \sin\alpha_w / f^2(\alpha_w) \geq 1/\beta, \qquad \text{(B-3)}$$

where β is a dimensionless parameter ($\beta \equiv 2k_0/\kappa_\omega$) that is basically a measure of the roughness height normalized to radio wavelength.

Figure B-1 shows the region (for $\nu > 0$) in ν-α space within which the mapping occurs, as defined by Eq. (B-2). Shown also are lines obtained from Eqs. (B-3); these along with the heavy shading indicate which regions of ν α space are most important for higher sea states and/or radar frequencies (i.e., higher values of β).

(c) Sign-change limits. The sign of the Doppler shift, ω_d, in (2) for each of the four terms of the integrand depends upon whether κ_{1x} and κ_{2x} are less or greater than zero. Thus, p-q space can be divided into three bands, as shown in Fig. B-2(a). The vertical, dashed lines delineating these regions are given by

$$-f^4(\alpha_{\substack{p\\n}})\cos\phi = \nu^4 \cos\phi\cos 2\alpha_{\substack{p\\n}} \pm \sin\phi\sqrt{2\nu^4 f^4(\alpha_{\substack{p\\n}}) - \nu^8\cos^2 2\alpha_{\substack{p\\n}} - f^8(\alpha_{\substack{p\\n}})}, \text{ and}$$

$$\nu^4 \cos\phi\cos 2\alpha_{\substack{p\\n}} \pm \sin\phi\sqrt{2\nu^4 f^4(\alpha_{\substack{p\\n}}) - \nu^8\cos^2 2\alpha_{\substack{p\\n}} - f^8(\alpha_{\substack{p\\n}})} = f^4(\alpha_{\substack{p\\n}})\cos\phi; \qquad \text{(B-4)}$$

The two values, α_p and α_n (going with the upper and lower signs, respectively, in these equations) originate because p and q have two solutions in terms of κ_1 and κ_2 (which are transformed to α, ν as):

$$p/k_0 = (\nu^4\cos\phi\cos^2 2\alpha \pm \sin\phi\sqrt{2\nu^4 f^4(\alpha) - \nu^8\cos^2 2\alpha - f^8(\alpha)})/f^4(\alpha), \text{ and}$$

$$q/k_0 = (\nu^4\sin\phi\cos^2 2\alpha \mp \cos\phi\sqrt{2\nu^4 f^4(\alpha) - \nu^8\cos^2 2\alpha - f^8(\alpha)})/f^4(\alpha). \qquad \text{(B-5)}$$

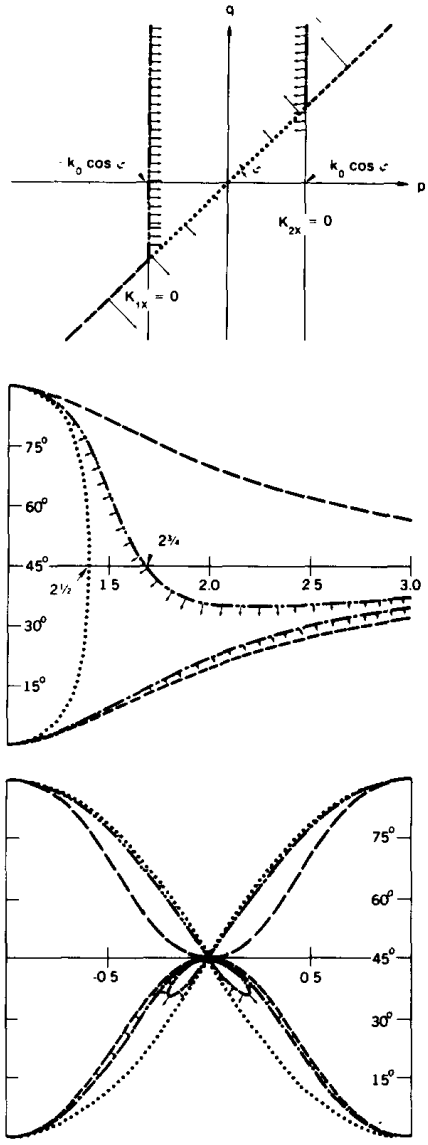

FIG. B-2. Plot showing how lines from $p-q$ space (upper) map onto $\nu-\alpha$ space for $1<|\nu|<3$ (middle) and $-1<\nu<+1$ (lower). A radar/wind direction of $\phi = 45^\circ$ is used for this example, and arrows show movement of boundaries as ϕ goes from 45° toward 90° (cross-wind case).

This further defines regions on the $p-q$ plane delineated by the dotted line with slope ϕ. This line is obtained by noting that the sign change is obtained at $\alpha = \alpha_j$, where one can solve the above two equations for the line to obtain $q/p = \tan \phi$.

For the sake of example, we show several of the relevant lines in Fig. B-2(b)

obtained from the above inequalities, mapped into $\nu-\alpha$ space; we employ $\phi = 45°$ for the curves of Fig. B-2. Furthermore, we indicate by arrows how these various lines collapse as $\phi \to 90°$, i.e., in the "crosswind" case.

Finally, we illustrate by chart form in Fig. B-3 how all of the four terms in the integrand of (2) map onto ν α space (again pictured for $\phi = 45°$). As can be seen, the entire four-term integrand over all p q space maps onto $\nu-\alpha$ space in a double-valued manner. This is important when one solves (4) numerically and attempts to take advantage of the various complementary symmetries of the mapping to reduce the computations. The solution of the inversion problem as formulated in the text is also clarified by understanding the mappings described here for solving the direct integral.

In effect, the coordinate system and transformation employed here accounts for radar/wave direction, ϕ, by changing the boundaries of the mapping (in both p q and ν α space), while keeping the waveheight spectra in the integrand invariant with ϕ. Transformations used by others (Lipa, 1977) keep the mapping boundaries constant, but include direction, ϕ, within the arguments of the waveheight spectra.

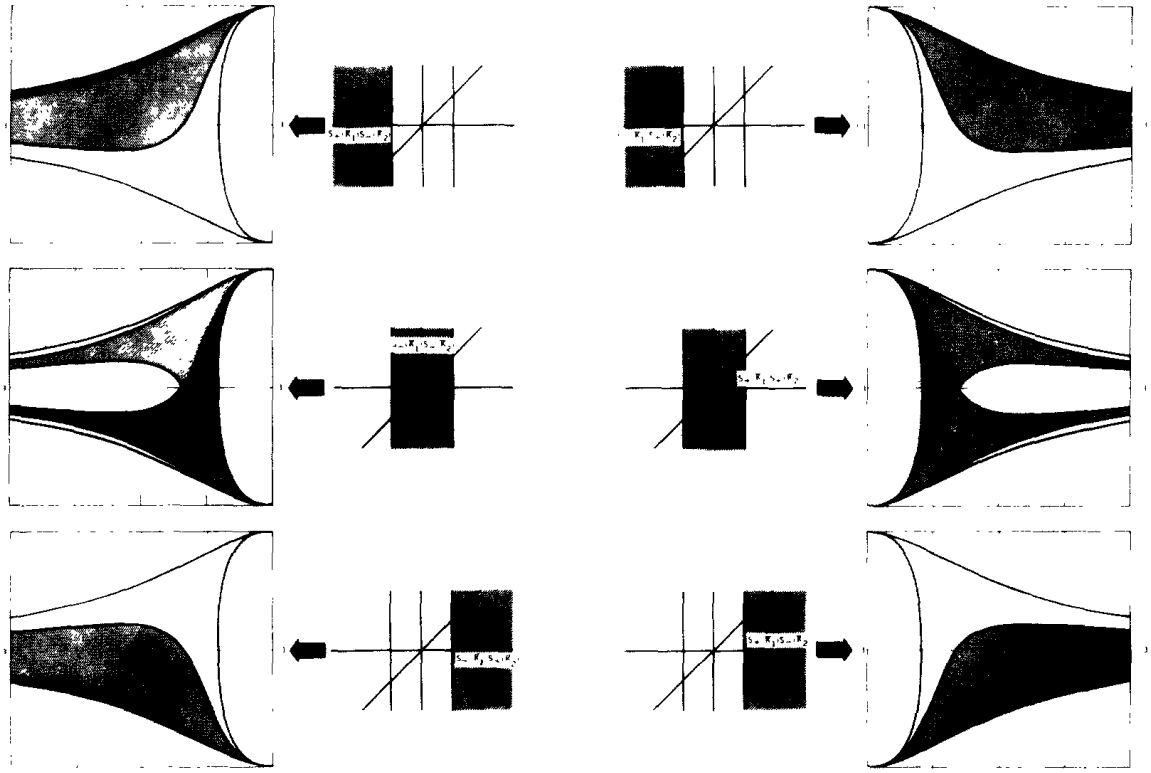

FIG. B-3(a). Plot showing how the various terms of the integrand of Eq. (2) map from p q space onto ν α space for $\phi = 45°$ and $1 < |\nu| < 3$.

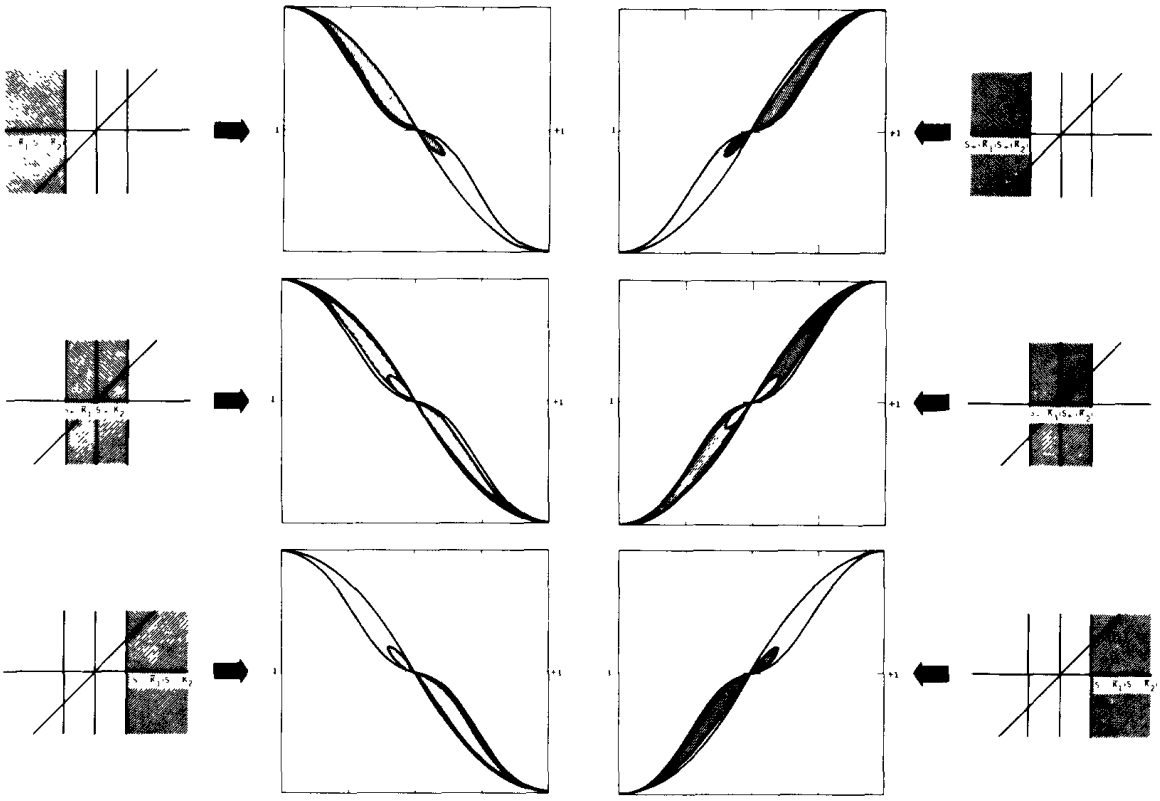

FIG. B-3(b). Plot showing how the various terms of the integrand of Eq. (2) map from p–q space onto ν–α space for $\phi = 45^\circ$ and $-1 < \nu < +1$.

References

Barrick, Donald E. (1971a), Theory of HF/VHF propagation across the rough sea, Parts I and II, *Radio Science* **6**, 517-533.

Barrick, Donald E. (1971b), Dependence of second-order sidebands in HF sea echo upon sea state, *IEEE G-AP International Symposium Digest*, (Sept. 21-24, 1971, Los Angeles, Calif.), pp. 194-197.

Barrick, Donald E. (1972a), First-order theory and analysis of MF/HF/VHF scatter from the sea, *IEEE Transactions on Antennas and Propagation*, Vol. AP-20, pp. 2-10.

Barrick, Donald E. (1972b), Remote sensing of sea state by radar in *Remote Sensing of the Troposphere*, V. E. Derr, ed., Chap. 12, U. S. Government Printing Office, Washington, D.C.

Barrick, Donald E., Headrick, James M., Bogle, Robert W., and Crombie Douglass D., (1974), Sea backscatter at HF: Interpretation and utilization of the echo, *IEEE*, Vol. 62, pp. 673-680.

Barrick, Donald E. (1973), The use of skywave radar for remote sensing of sea states, *Marine Technol. Soc. J.* **7(1)**, 29-33.

Barrick, Donald E. (1977), Extraction of wave parameters from measured HF radar sea-echo Doppler spectra, *Radio Science* 12, No.3.

Crombie, Douglass D. (1955), Doppler spectrum of sea echo at 13.56 Mc/s, *Nature* **175**, 681-682.

Hasselmann, Klaus (1971), Determination of ocean wave spectra from Doppler radio return from the sea surface, *Nature Physical Science* **229**, 16-17.

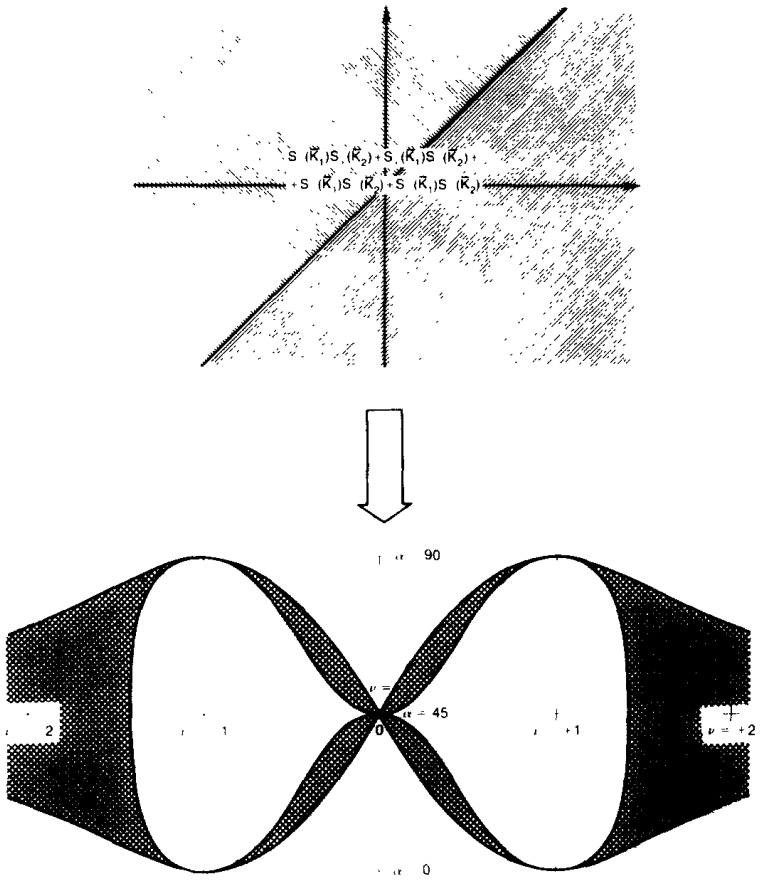

FIG. B-3(c). Total combination of mappings of previous two figures.

Kinsman, Blair (1965) *Wind Waves*, Prentice-Hall, Inc., Englewood Cliffs, New Jersey.

Lipa, Belinda J. (1977), Derivation of Directional ocean wave spectra by integral inversion of second order radar echoes, *Radio Science* 12, No. 3.

Phillips, Owen M. (1966), *Dynamics of the Upper Ocean*, Cambridge University Press, London, England, pp. 109-139.

Rice, Stephen O. (1951), Reflection of electromagnetic waves from slightly rough surfaces, in *Theory of Electromagnetic Waves*, M. Kline ed., Interscience Publishers, New York, pp. 351-378.

Stewart, Robert H. (1971), *Higher order scattering of radio waves from the sea*, IEEE G-AP International Symposium Digest, (Sept. 21-24, 1971, Los Angeles, Calif.), pp. 190-193.

Teague, Calvin C., Tyler, G. Leonard, and Stewart, Robert H. (1975), The radar cross section of the sea at 1.95 MHz: Comparison of in-situ and radar determinations, *Radio Science* **10**, 847-852.

Tyler, G. Leonard, Teague, Calvin C., Stewart, Robert H., Peterson, Allen M., Munk, Walter H., and Joy Joseph W., (1974), Wave directional spectra from synthetic aperture observations of radio scatter, *Deep Sea Research* **21**, 989-1016 (Pergamon Press, printed in Great Britain).

Valenzuela, Gaspar R. (1974), The effect of capillarity and resonant interactions on the second-order Doppler spectrum of radar sea echo, *Geophys. Res.* **79**, 5031-5037.

Received 6 December 1976; revised 10 March 1977